Batteries & Supercaps

Research Article
doi.org/10.1002/batt.202400822

Chemistry Europe
European Chemical Societies Publishing

www.batteries-supercaps.org

Unraveling the Effects of Redox-Active Electrolytes on Carbon Electrodes in Li-Ion Capacitor

Adam Mackowiak,* Przemyslaw Galek,* Paweł Jezowski, and Krzysztof Fic*

The quest for efficient and sustainable energy storage solutions has generated significant interest in lithium-ion capacitors (LICs) due to their balanced power and energy characteristics. This study explores the performance of carbon electrodes in LICs prelithiated with a redox-active electrolyte containing lithium thiocyanate (LiSCN). The impact of thiocyanate on electrode performance is investigated utilizing step potential electrochemical spectroscopy (SPECS) and the galvanostatic intermittent titration technique (GITT). In the studied conditions, the thiocyanate reaction proceeds with an efficiency of ≈81%, resulting in a capacity of 301 mAh g^{-1} for the positive electrode. Notably, the presence of thiocyanates significantly reduces the resistance of the negative electrode by 30%. Therefore, the addition of LiSCN facilitates lithium intercalation in the negative graphite electrode, enhancing capacity and reducing resistance. The SPECS technique reveals distinct intercalation stages and improved ion diffusion, while GITT confirms these findings with diffusion coefficients. Overall, the study demonstrates the efficacy of using redox-active electrolytes in LICs, presenting a viable path for optimizing their performance in future applications.

1. Introduction

In the realm of energy storage, the quest for efficient and sustainable solutions continues to drive innovation and research. Electric double-layer capacitors (EDLCs), due to their high power (≈10 kW kg^{-1}) and long lifespan (≈1 million cycles), find applications in fields such as automotive, electronics, renewable energy, and public transportation.[1–4] However, EDLCs have significantly lower specific energy (≈10 Wh kg^{-1}) compared to lithium-ion batteries (≈250 Wh kg^{-1}).[5,6] While lithium-ion batteries are the most popular energy storage solutions currently available, their short lifespan (1000 cycles) and low specific power (<1 kW kg^{-1}) necessitate the exploration of new alternatives.[7,8] One such alternative is lithium-ion capacitors (LICs), which offer optimal power (5 kW kg^{-1}) and energy (≈50 Wh kg^{-1}) values while maintaining a long lifespan (≈100,000 cycles).[9,10] LICs are emerging as an attractive option for applications including automotive regenerative braking, spacecraft power supply, renewable energy, and small portable electronics.[11–14] LICs offer a promising solution poised to meet the evolving demands of modern energy storage requirements.

In constructing LICs, carbon-based electrodes are predominantly used, making them lightweight and cost-efficient.[15] The negative electrode in capacitors can be composed of materials such as reduced graphene oxide, biomass-derived hard carbons, transition metal dichalcogenides, and metal oxides like $Li_5Ti_5O_{12}$, TiO_2, and Nb_2O_5.[16–19] Most of the materials mentioned possess a layered structure, allowing lithium ions to penetrate their structure and deposit between these layers. However, graphite is considered an ideal anode material for LICs due to its flat and low Li-insertion potential of ≈0.1 V as well as its high theoretical capacity of 372 mAh g^{-1}.[20] Positive electrodes in LICs can consist of B and N co-doped carbon nanofibers, carbon nanotubes, and graphene.[21–23] Activated carbon (AC) dominates as a positive electrode material in LIC research based on the energy-storage mechanism of surface adsorption, as it exhibits high surface area (≈3000 m^2 g^{-1}), excellent conductivity (≈60 S m^{-1}) and good chemical stability.[24,25]

However, LICs face a structural obstacle: a prelithiation process must be performed for them to function. Currently, several methods are known in the literature that enables an efficient prelithiation process, such as those using an additional lithium electrode, sacrificial material, or a concentrated lithium electrolyte.[9,26–28] Recently, another method has emerged, using redox-active salts in the electrolyte.[29] This approach involves oxidizing redox salts on the positive electrode during the first charging cycle, facilitating efficient intercalation of the negative electrode. It is crucial for the reaction to occur at a potential values lower than the electrolyte decomposition potential and to be irreversible. The oxidation reaction of redox salts primarily occurs on the positive electrode—but how does the presence of this reaction affect the performance of the negative electrode?

A. Mackowiak, P. Jezowski, K. Fic
Poznan University of Technology
Institute of Chemistry and Technical Electrochemistry
Berdychowo 4, 60-965 Poznan, Poland
E-mail: adam.mackowiak@put.poznan.pl
krzysztof.fic@put.poznan.pl

P. Galek
Department of Inorganic Chemistry I
Technische Universität Dresden
Bergstraße 66, 01069 Dresden, Germany
E-mail: przemyslaw.galek@tu-dresden.de

Supporting information for this article is available on the WWW under https://doi.org/10.1002/batt.202400822

Redox-active electrolytes offer significant advantages for LICs, such as enhanced capacity and improved energy density through additional faradaic reactions.[30] However, these benefits come with trade-offs and limitations. One major concern is the increased complexity of electrochemical reactions, which can lead to side reactions, accelerated electrolyte degradation, and the formation of an unstable solid electrolyte interphase (SEI). Additionally, redox-active species may introduce higher self-discharge rates and lower Coulombic efficiency, affecting long-term stability.[31] The solubility and diffusion of redox-active compounds can also impact electrode performance, leading to capacity fading over extended cycling. Balancing these factors is crucial for optimizing the practical application of redox-active electrolytes in LICs.[32]

There are several electrochemical techniques commonly used to assess the performance of the electrode, such as galvanostatic cycling with potential limitation (GCPL), cyclic voltammetry, and potentiostatic electrochemical impedance spectroscopy (PEIS).[33–35] These techniques provide valuable information about capacity, resistance, efficiency, cyclability, and power and energy output (at the relevant device level).[36] To determine the diffusion coefficient parameter, the most commonly chosen techniques are the galvanostatic intermittent titration technique (GITT) and the potentiostatic intermittent titration technique.[37,38] However, due to the sensitivity of the lithium intercalation and deintercalation processes in the graphite structure, the use of GITT appears to be a better and more reliable solution.[39,40]

In 2015, the step potential electrochemical spectroscopy (SPECS) technique for detailed characterization of energy storage systems was demonstrated.[41] The SPECS technique has primarily been used for electrochemical capacitors (ECs).[42] However, with appropriate reasoning, it has also been applied to provide detailed descriptions of battery systems.[43] Combining the SPECS and GITT techniques represents a powerful tool for analyzing processes occurring in energy storage devices.

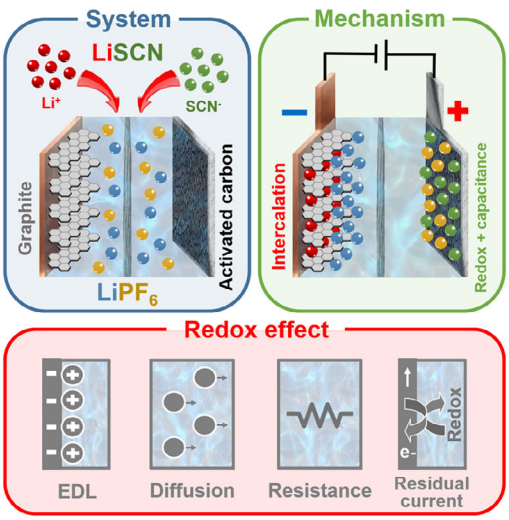

Figure 1. Schematic representation of the study with the assembly of hybrid metal-ion capacitors containing a redox-active electrolyte.

In this article, the SPECS technique was utilized to investigate the processes occurring on the carbon electrodes of an LIC, which were prelithiated using an electrolyte containing a redox salt additive (**Figure 1**). This additive was lithium thiocyanate (LiSCN). The capacitor electrodes were examined both in half-cells and in the full system configuration. Subsequently, the results obtained from SPECS were compared with other commonly used techniques such as PEIS, GCPL, and GITT.

2. Experimental Section

2.1. Electrolyte

Lithium hexafluorophosphate ($LiPF_6$) and lithium thiocyanate hydrate ($LiSCN \cdot xH_2O$) were procured from Sigma–Aldrich (Merck; Germany) and subjected to a desiccation process under vacuum at 120 °C for 1 week. Lithium thiocyanate hydrate underwent a pre-drying procedure at 130 °C employing a liquid nitrogen cold trap to remove water excess. Anhydrous solvents, ethylene carbonate (EC), and dimethyl carbonate (DMC) were obtained from Sigma–Aldrich. The electrolyte for the cells consisted of a 1 molar solution of $LiPF_6$ dissolved in a mixture of EC and DMC in a 1:1 volumetric ratio. For the redox electrolyte, a one molar solution of $LiPF_6$ in a mixture of EC and DMC was utilized, supplemented with a calculated amount of LiSCN salt. The quantity of thiocyanate salt added to the electrolyte was determined based on the mass of the negative electrode and its theoretical capacity. The conductivity of the electrolyte without the redox component measured 13.01 mS cm^{-1}, while the electrolyte with thiocyanate salt exhibited a conductivity of 10.88 mS cm^{-1}. Conductivity assessments were conducted at room temperature (21 °C) using a two-electrode Swagelok system with a spacer, employing PEIS. 600 μL of the prepared electrolytes were utilized to saturate the separators during the assembly of the electrochemical cells. All chemicals were stored in a glovebox (MBraun; Germany) to maintain an inert environment.

2.2. Electrode Material

The negative electrode of the hybrid LIC was fabricated utilizing copper foil coated with artificial graphite (total thickness = 100 μm), sourced from Customcells. As for the positive electrode, a self-standing electrode composed of Kuraray YP80F (80%), polytetrafluoroethylene (10%), and carbon black C65 (10%) (total thickness = 114 μm) was used. The positive electrode surface area was 1558 $m^2 g^{-1}$. The microtextural properties of the positive electrode were assessed using the Brunauer–Emmett–Teller isotherm method at 77 K, employing N_2 as an adsorbate (ASAP 2460; Micromeritics; USA). Before adsorption/desorption procedures, samples underwent flushing at 350 °C for 12 h under continuous helium flow, followed by further degassing at 25 °C for 5 h under vacuum conditions.[44] Before the cell assembly, both negative and positive electrodes were dried for 24 h at 120 °C using a vacuum chamber.

The reference electrode consisted of metallic lithium obtained from Sigma–Aldrich.

2.3. Cell Assembly

Circular electrodes with a diameter of 16 mm and a surface area of 2 cm^2 were obtained from both positive and negative electrode materials using EL-Cut (EL-CELL; Germany) The active mass ratio between the electrodes was maintained at ≈1:1. Before cell assembly, the electrolyte was freshly prepared. The positive and negative electrodes were then positioned in an electrochemical cell with reference electrode (ECC-REF; EL-CELL), separated by two glass fibre discs with a diameter of 18 mm (GF/D; Whatman; UK), each saturated with 600 μL of electrolyte. The reference electrode was inserted into the reference pinhole using an ECC loader (EL-CELL). For half-cell measurements, the counter and reference electrodes, consisting of metallic lithium, were shaped as discs with a diameter of 16 mm. All assembly procedures were performed within a glovebox.

2.4. Electrochemical Investigation

Electrochemical measurements were conducted using a multichannel galvanostat/potentiostat (VMP-3; Biologic; France) under the control of EC-Lab software at room temperature (21 °C). The SPECS measurement involved applying a sequence of potentiostatic hold periods, controlled by chronoamperometry (CA): every 1 mV to 0.01 V *vs.* Li/Li^+ for 10 min. This protocol was designed to comprehensively monitor system changes, particularly emphasizing potential regions below 0.3 V, where individual intercalation/deintercalation events occur. Furthermore, a GITT examination was performed on each electrochemical system to determine the diffusion coefficient. Cells underwent testing with the C/20 current using the GCPL technique, involving a series of charging and discharging steps by delivering the current for an hour followed by a 1 h hold period to achieve complete intercalation.

2.5. Step Potential Electrochemical Spectroscopy

This method has recently been introduced into the realm of EDLCs[41] and battery systems.[43] The fundamental concept underlying SPECS involves subjecting the cell to a series of gradual changes in potential (referred to as steps), followed by periods of rest. These rest intervals are sufficiently long to allow the current response to reach an equilibrium state. By employing small step changes, SPECS facilitates the completion of maximum storage capacities while simultaneously offering insights into various factors of energy storage mechanisms. The total current (I_T) recorded during a specific potential step can be divided into distinct components, namely those associated with electric double-layer (EDL) formation (I_{EDL}), diffusion-limited processes (I_D), and residual processes (I_R), as expressed by Equation (1).[45]

$$I_T = I_{EDL} + I_D + I_R \quad (1)$$

In the context of ECs, the description of electric double-layer (EDL) formation current (I_{EDL}) can be further elaborated to distinguish between the current associated with electrode porosity (referred to as pore-related current, I_P) and the current about electrode geometry, specifically the outer electrode surface (geometric current, I_G). However, in the case of battery systems, this differentiation becomes inconsequential due to the predominance of charge storage mechanisms primarily driven by redox reactions. Thus, it is clearer to simply characterize it as EDL current. Therefore, considering the influence of rest time (t) and potential step (ΔE), it becomes feasible to compute additional components such as resistance (R_{EDL}), differential capacitance (C_{EDL}), diffusion parameter (B), and residual current (I_R), culminating in the formulation of the final equation (**Equation (2)**).

$$I_T = \frac{\Delta E}{R_{EDL}} \exp\left(-\frac{t}{R_{EDL} + C_{EDL}}\right) + \frac{B}{t^{0.5}} + I_R \quad (2)$$

I_R refers to the steady-state current that remains after a potential step is applied to the electrochemical system and the transient current has decayed. This residual current is typically constant because it represents the current flowing in the system when the electrochemical processes have reached a steady state. Nevertheless, in instances where a redox reaction transpires at a specific potential, the I_R current will proportionately escalate.

By collating the computed system components, a comprehensive depiction of system operation can be worked out. Hence, SPECS emerges as a rapid and efficacious tool for delineating the stability of electrode materials, assessing ionic mobility within the electrolyte, quantifying the equivalent series resistance (ESR) of electrode materials, and even optimizing cell engineering.[46,47]

2.6. Galvanostatic Intermittent Titration Technique

Unlike SPECS, GITT is a technique in which a current pulse is applied to the system, and its potential response is measured. GITT is a well-known and commonly used technique primarily for determining the diffusion coefficient of energy storage systems.[39] To calculate the diffusion values, the Weppner and Huggins equation is often employed.[48] However, for precise determination of the lithium-ion diffusion coefficient in a system with graphite electrode, the modified Equation (3) is applied.[40]

$$\tilde{D} = \frac{4}{9\pi}\left(\frac{E_4 - E_0}{E_2 - E_1}\right)^2 \frac{r_2^p}{t_p} \text{ for } \left(\tau \ll \frac{L^2}{\tilde{D}}\right) \quad (3)$$

In Equation (3), the symbol $\tilde{D}$ represents the diffusion coefficient [$m^2\ s^{-1}$], τ is the interval time from charging to discharging (without relaxation phase) [s], and L is the sample thickness [m]. The potential response observed during GITT comprises five distinct phases: starting from the initial potential (E_0), transitioning through the voltage jump (IR drop; $E_1 - E_0$), progressing to the increment phase ($E_2 - E_1$), further proceeding through the subsequent IR drop ($E_3 - E_2$), and ultimately reaching the phase of final resting potential (E_4) (Figure 1). Utilizing this equation, along with the potential response data, the values of t_p (pulse duration) and r_p (particle radius – graphite 9 μm; AC 5 μm) allow the lithium diffusion coefficient to be determined (**Figure 2**).

Research Article
doi.org/10.1002/batt.202400822
Chemistry Europe
European Chemical Societies Publishing

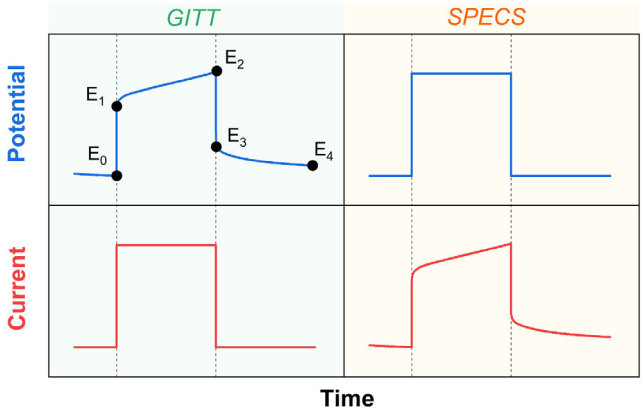

Figure 2. Schematic comparison of the single galvanostatic intermittent titration technique (GITT) pulse and step potential electrochemical spectroscopy (SPECS) pulse.

3. Results and Discussion

In light of recent reports in the literature on one-step preintercalation in hybrid metal-LICs, this study investigated the impact of redox-active electrolytes on the performance of individual electrodes in a LIC.[29] To thoroughly examine the effects of thiocyanates, their electrochemical behaviour during standard constant current charging and discharging of the system was first demonstrated. **Figure 3**a illustrates the effect of thiocyanate salt in the solution on the performance of the positive electrode.

By applying a current of C/20 (where C corresponds to the theoretical full charge capacity of the graphite electrode, 372 mAh g^{-1}), the system without SCN^- anions (yellow curve) exhibits a purely capacitive behaviour. The capacity for such charging up to 4.5 V is 71 mAh g^{-1}, indicating a deficit of 301 mAh g^{-1} required to fully charge the graphite electrode. To address this capacity deficiency, a precisely calculated amount of thiocyanate was added to the electrolyte, which increased the capacity to 372 mAh g^{-1} (red curve), thus matching the graphite electrode full charge capacity. The presence of thiocyanates creates a potential plateau around 3.5 V, which limits the potential increase of the positive electrode, allowing it to accumulate sufficient capacity without exceeding the cut-off potential (i.e., 4.5 V). As observed, during discharge, the curve displays a more capacitive character, suggesting that most thiocyanates underwent irreversible reactions during the initial charge.

Subsequently, the negative electrode (graphite) was studied in a half-cell configuration with and without the addition of thiocyanate salt (Figure 3b). The system with the added salt achieved a higher first-cycle capacity (399 mAh g^{-1}; green curve) compared to the system without the addition (383 mAh g^{-1}; purple curve). However, a part of this capacity was utilized to form the SEI layer, resulting in a higher irreversible capacity (47 mAh g^{-1}) compared to the system without the addition (36 mAh g^{-1}). Nonetheless, both systems exhibited very similar performance, with distinct intercalation stages observed, suggesting that the SCN^- anions did not have a significant impact on the process of lithium intercalation into the graphite structure.

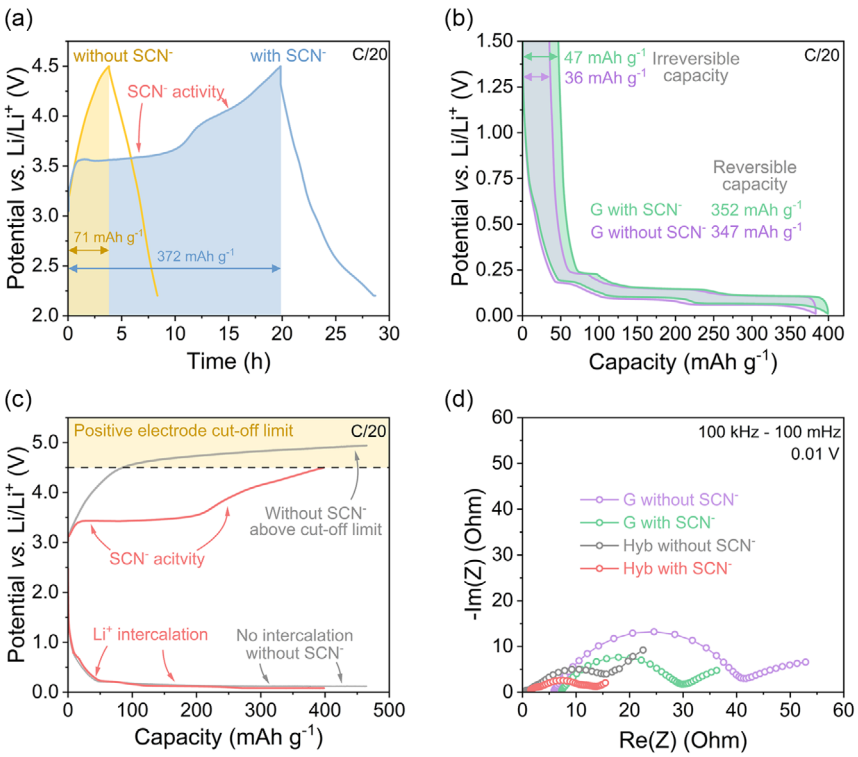

Figure 3. Comparison of charging and discharging curves for systems with and without electroactive additive in electrolyte a) half-cells with activated carbon, b) half-cells with graphite, c) full hybrid cells, and d) impedance spectroscopy results for graphite electrodes in half-cells and full hybrid cells.

In the subsequent phase of the study, two hybrid capacitor systems were assembled, with graphite serving as the negative electrode and AC as the positive electrode. In one of these systems, LiSCN salt was added to the electrolyte. As shown in Figure 3c, the system without thiocyanate additives quickly reached the cut-off potential of the positive electrode, and the curve flattened, indicating an electrochemical reaction that decomposes the electrolyte. Meanwhile, no distinct intercalation stages were observed at the negative electrode, resulting in the system not achieving the expected capacity. The addition of SCN^- salt, as observed in the half-cell experiments, mitigated the increase in the positive electrode potential, acting as a charge-balancer and facilitating the intercalation of lithium cations into the graphite structure. Additionally, it is likely that lithium ions participated in reactions and did not adversely affect electrolyte conductivity, as the cation balance was maintained relative to a standard electrolyte. This approach confirms the effectiveness of the one-step assembly approach in LICs.

Subsequently, it was decided to investigate the resistances using the PEIS technique for the electrodes in their fully charged state. For the positive electrodes, this was at a potential of 4.5 V, while for the negative electrodes it was at a potential of 0.01 V. Figure S1 compares the performance of the positive electrodes. The ESR for both systems is similar (5 ohms for the system with SCN^- anions and 6 ohms for the system without SCN^-), as both were constructed with the same electrode materials. However, the resistance represented by the semicircle size for the SCN^- system is significantly higher. This indicates an increased charge transfer resistance at the electrode/electrolyte interface, which is attributed to charge separation at the phase boundary or ion diffusion resistance in the electrolyte, particularly near the electrode surface.[49] This suggests that the presence and reaction of thiocyanate anions may hinder the charge transfer at the positive electrode during the first cycle.

In contrast, for the negative electrodes (Figure 3d), the presence of SCN^- ions positively affects the resistance values in the system. This difference may be due to the reduction of some thiocyanate anions on the negative electrode surface, forming a less resistive SEI layer that facilitates the transport of lithium ions into the graphite structure. When comparing the performance of the negative electrodes in full hybrid systems, it should be noted that the response from the Stern layer in the spectra for both systems was comparable; however, the addition of SCN^- ions did not influence the thickness of the Stern layer. It should be considered that the SCN^--containing system was fully intercalated, which results in lower resistance values in the semicircle.

To effectively analyze the results obtained from the SPECS technique, it is essential first to consider the parameters that can be extracted using this powerful tool. The total current can be divided into EDL current, diffusive current, and residual current. The area under the current curves allows for the calculation of capacities attributed to EDL, diffusion, and residual effects. The "*SPECSFit*" software can further refine these equations to yield detailed values such as the diffusion parameter, time constant, and EDL layer resistance. The current associated with EDL layer formation can be further categorized into pore-related current and geometric current. In the context of EDLCs, pore-related current relates to the formation of the EDL layer within the porous materials of the positive electrode. For graphite, this should be considered as the ion-accessible space between graphene layers. Geometric current in EDLCs refers to the outer electrode surface that is easily accessible to the electrolyte, whereas for graphite systems, it describes the edges of the graphene layers. In the studies conducted, however, the distinction between porous and geometric components was not made, to simplify the analysis by considering them as related to double-layer formation. Applying an appropriate potential step is crucial in SPECS studies. A very slow potential step was used in the experiments to achieve the most accurate current curve, with a 1 mV potential step every 10 min. This long interval ensures equilibrium of the current curve, though it extends the experiment duration. The 1 mV step is particularly important for capturing changes in the graphite electrode system, where potential differences between intercalation stages are marginal.

The SPECS studies began by examining half-cells with AC. In this case, systems with and without the addition of LiSCN were compared, as shown in **Figure 4**.

Initially, the total current was converted to a total specific capacity. A distinct signal from the thiocyanate reaction at a potential of 3.4 V was observed. This potential is slightly lower than the reaction potential observed in the previous galvanostatic charge study. This occurs because the SPECS study is much slower and more detailed, allowing for the capture of capacity changes much earlier. Here, it is also important to note that the electrolyte begins to decompose at around 4.3 V, making it crucial for ageing systems not to exceed this potential. Figure 4b illustrates that the specific EDL capacity is comparable for both systems above 3.6 V. However, during the SCN reaction, an increase in EDL capacity is observed, likely due to the attraction of SCN^- ions by the positive electrode of the cell. The residual capacity curve (Figure 4c) primarily reflects the total specific capacity, which is consistent as the faradaic reaction of the thiocyanate anion predominates here. The capacity of the diffusive layer (Figure 4d) is negligible but, as expected, is higher for the system with thiocyanates. This is due to the presence of additional ions in the system. The EDL layer resistance (Figure 4e) is higher for the system without thiocyanates, indicating a better-organized double-layer structure for the system with thiocyanates. The time constant curve (Figure 4g) is comparable to the EDL resistance, meaning the system requires more time to settle and adsorb ions on the surface of the positive electrode. Figure 4h,l compile the capacities: total capacity, EDL capacity, diffusive capacity, and residual capacity. As shown, the residual capacity has the most significant impact on the redox electrolyte system (94%), which is logical due to the electrochemical reaction. Moreover, for the system without SCN^-, the residual capacity also has the most significant impact. This result is somewhat misleading, but closer examination of the EDL curve reveals that EDL storage predominates initially, and towards the end, when electrolyte decomposition processes occur, the capacity from the residual current increases. Figure S2, Supporting Information, describes other parameters obtained during SPECS technique measurement. One of the more important curves is the fitting curve (Figure S2b, Supporting Information), which shows that

Research Article
doi.org/10.1002/batt.202400822
Chemistry Europe
European Chemical Societies Publishing

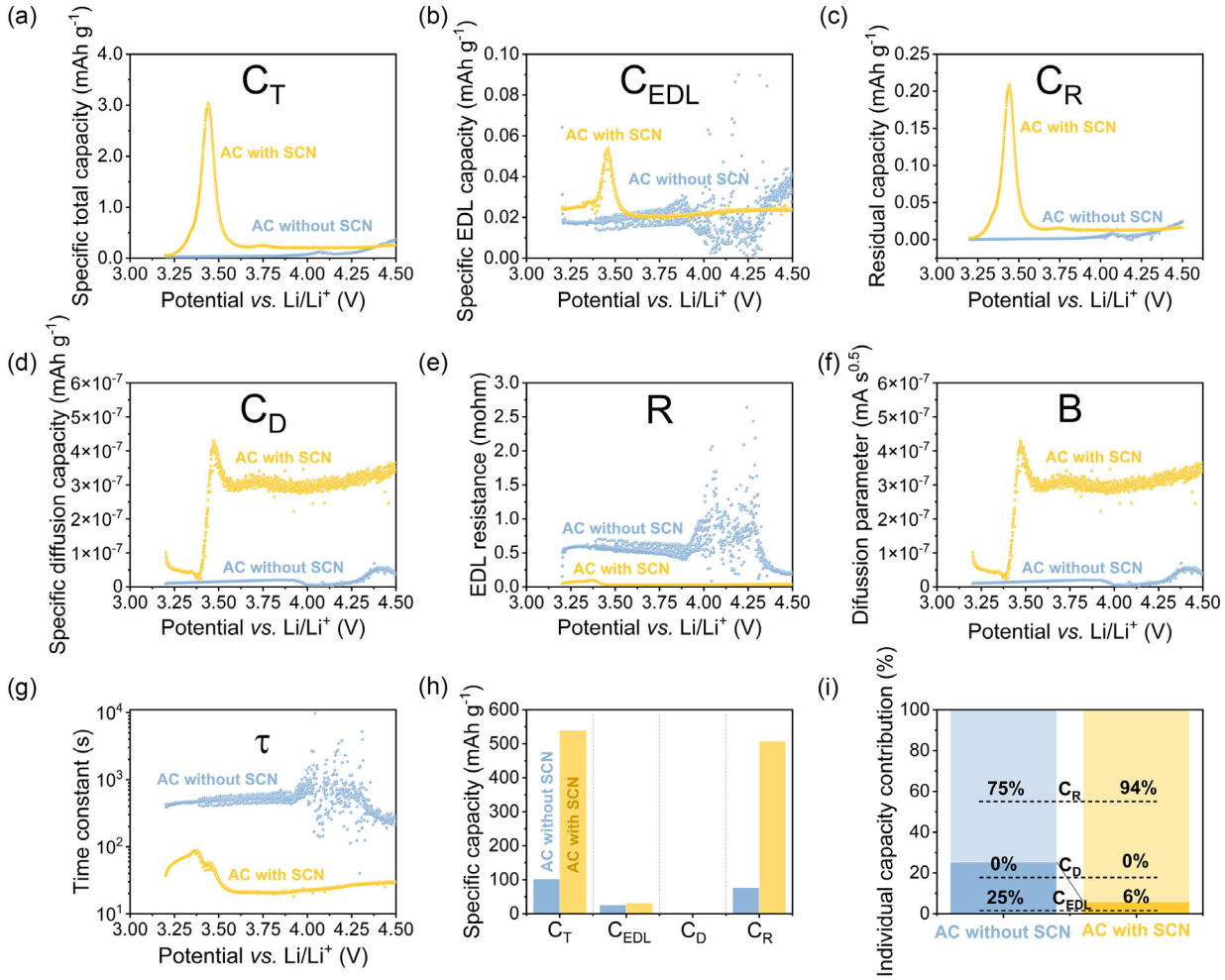

Figure 4. SPECS results of activated carbon-based half-cells with thiocyanate salt as an electrolyte additive a) specific total capacity (C_T), b) specific EDL capacity (C_{EDL}), c) residual capacity (C_R), d) specific diffusion capacity (C_D), e) EDL resistance (R), f) diffusion parameter (B), g) time constant (τ), h) specific capacity comparison, and i) individual capacity contribution.

the error of the fitted curves is marginal, and the fitting reflected a good correlation coefficient of more than 99%.

Next, a SPECS study was conducted for two graphite systems in half-cells (**Figure 5**).

Again, one system had a dissolved thiocyanate electrolyte, while the other did not. In both cases, intercalation proceeded successfully, with distinct intercalation stages visible (Figure 5a). However, for the SCN system, the third stage is more pronounced (the signal is narrower and higher) than for the system without the electrolyte additive. Moreover, the individual intercalation stages occur slightly but at a higher potential than in a traditional lithium-graphite half-cell. Interestingly, during deintercalation, the curves of both systems overlap, suggesting changes only during the charging of the graphite electrode (Figure S3). A slight increase in capacity at a potential of about 0.75 V can also be observed, suggesting the formation of more SEI in the system with thiocyanates (Figure 5a). The capacity of the EDL layer in this case should be negligible (Figure 5b). Only at the beginning and end of the charging cycle was capacity originating from the EDL observed, which is more related to the attraction of cations to the electrode surface rather than actual EDL storage due to the lack of pores and the small specific surface area of graphite (about 1 m^2 g^{-1}). The capacity associated with the redox reaction is dominant here due to the lithium intercalation process, making the residual capacity curve very close to the total specific capacity curve (Figure 5c). The diffusive capacity is, of course, marginal (Figure 5d); however, in the beginning, diffusion is higher for the system without SCN, but from the moment reactions related to SEI formation occur, there is a significant increase in diffusion in the thiocyanate system. This is another sign suggesting that thiocyanates are responsible for the SEI layer formation. The resistance of the EDL layer follows a characteristic pattern, where initially, lithium ions diffuse towards the negative electrode, and the resistance is high (up to 18 mOhm). However, as the process progresses, the electrical double-layer resistance drops practically to zero. Comparing the capacities obtained for both systems, as in the galvanostatic studies, the capacity for graphite with thiocyanates is slightly higher than for the system without. However, the percentage values in comparison between the individual components are comparable for both systems. Figure S4a, Supporting Information, shows how dominant the residual current is, and the fitting curve is also very high, above 99%.

Research Article
doi.org/10.1002/batt.202400822
Chemistry Europe
European Chemical Societies Publishing

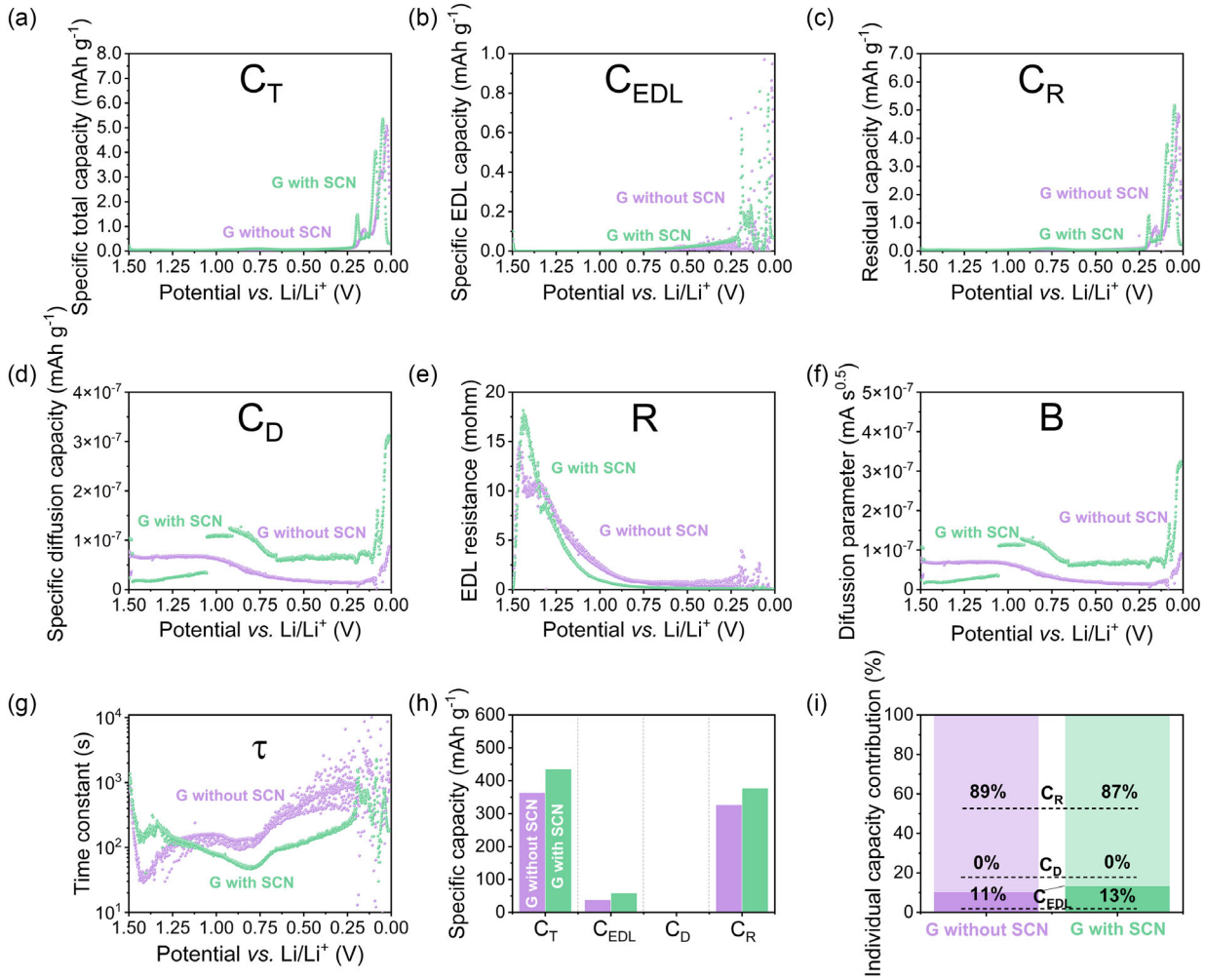

Figure 5. SPECS results of graphite-based half-cells with thiocyanate salt as an electrolyte additive a) specific total capacity (C_T), b) specific EDL capacity (C_{EDL}), c) residual capacity (C_R), d) specific diffusion capacity (C_D), e) EDL resistance (R), f) diffusion parameter (B), g) time constant (τ), h) specific capacity comparison, and i) individual capacity contribution.

In the next step, SPECS studies were conducted in a three-electrode system, where graphite was the negative electrode, AC was the positive electrode, and metallic lithium was the reference electrode (**Figure 6**).

In this case, the performance of negative electrodes in full hybrid systems with and without the addition of thiocyanates was compared. The hybrid without thiocyanates was not fully intercalated, as previously explained during the discussion of Figure 3. Nevertheless, it was decided to show the performance of this cell for comparison purposes with the hybrid assembled using the one-step assembly approach. Through the SPECS technique, the successive intercalation steps of the hybrid system with SCN (Figure 6a) can be observed. The system without thiocyanates cannot surpass the graphite potential of 0.5 V, indicating a lack of lithium intercalation process. The capacity originating from the EDL in the hybrid without SCN is negligible, while in the SCN hybrid, it increases at the end of the charging cycle and corresponds to the intercalation stages (Figure 6b). Interestingly, the diffusion value in the hybrid system with SCN starts to increase exponentially from a potential of 0.5 V, suggesting heightened ion activity (Figure 6d). The EDL layer resistance is similar for both systems (Figure 6e), which is related to ion movement in the initial phase towards the negative electrode. Only later, when the appropriate energy barriers are overcome, does intercalation occur, and the resistance associated with EDL layer formation decreases. Comparing the individual capacity values (Figure 6h,l), it can be noted that for the system without SCN, 98% of the capacity is related to reactions within the system, but not intercalation rather, electrolyte decomposition. In contrast, for the system with SCN, the capacity arising from the reduction reaction constitutes 90% of the individual components. However, the EDL capacity accounts for 10%, so it is important to remember that the operation of the negative electrode is not only intercalation. Figure S5, Supporting Information, shows a very good fitting curve for the system with SCN, but for the system without thiocyanates, the error is significant. This suggests that the SPECS technique can be successfully used only for systems where no large fluctuations in potential and no violent reactions occur.

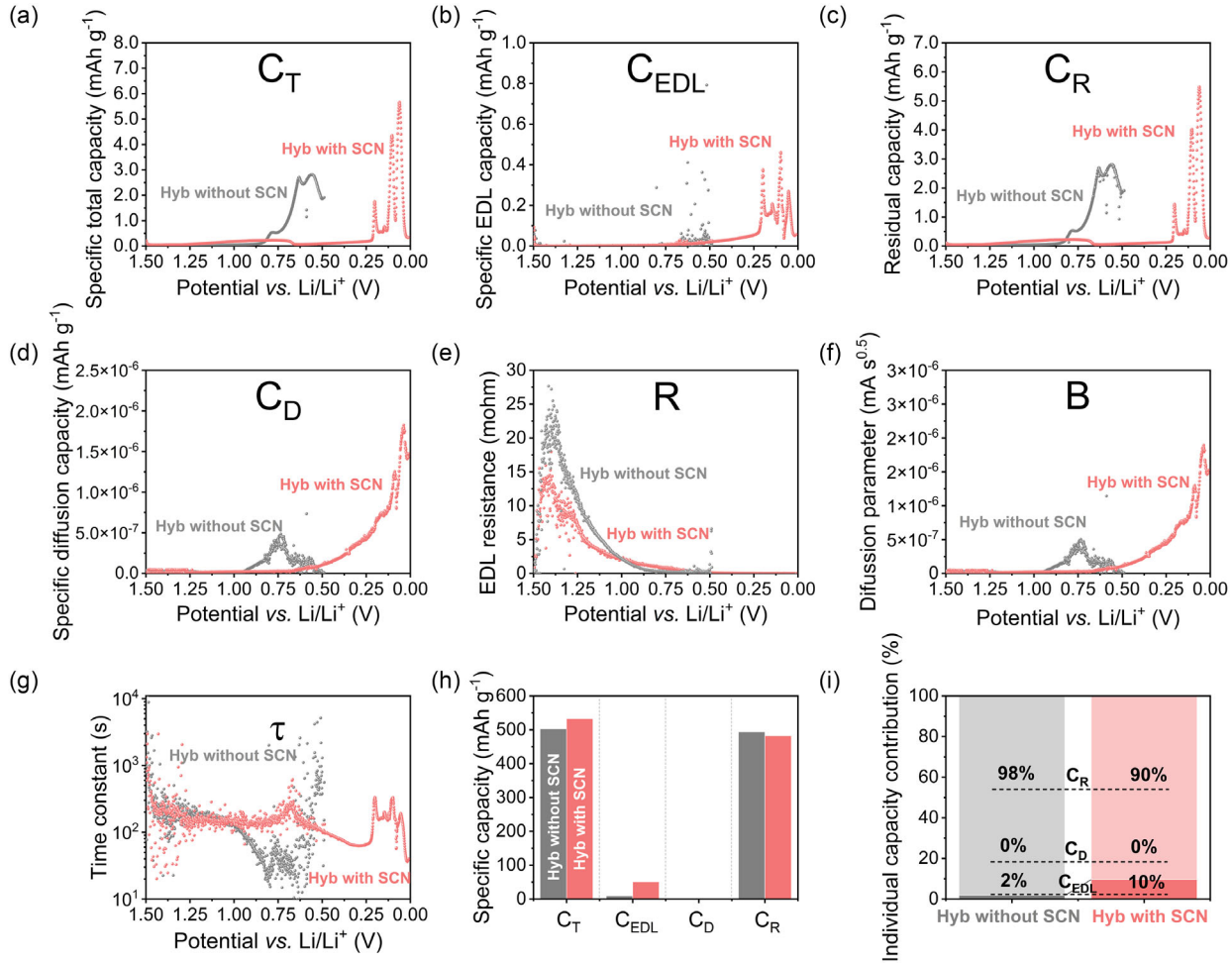

Figure 6. SPECS results of full cells using graphite and activated carbon with thiocyanate salt as an electrolyte additive a) specific total capacity (C_T), b) specific EDL capacity (C_{EDL}), c) residual capacity (C_R), d) specific diffusion capacity (C_D), e) EDL resistance (R), f) diffusion parameter (B), g) time constant (τ), h) specific capacity comparison, and i) individual capacity contribution.

In the final comparison of SPECS results, a graphite-lithium half-cell with SCN was compared to a fully intercalated hybrid using the one-step assembly approach (**Figure 7**). It is common in scientific studies to test electrodes in half-cells without considering their performance in full systems which may differ. This comparison aims to highlight the differences in the performance of the graphite electrode, where theoretically the same processes should occur. However, one system has a metallic electrode with constant potential as a counter electrode, whereas the other has an active carbon electrode with additional oxidation reactions as a counter electrode.

Comparing the total specific capacity values for both systems shows that the capacities responsible for individual intercalation stages overlap, suggesting that the electrodes operate in the same manner (Figure 7a). However, it should be noted that in the SCN hybrid, a much larger capacity is utilized for SEI formation. In practice, this means that the simultaneous reaction occurring at the positive electrode affects the SEI layer formation, as the oxidation of thiocyanates is not observed in the lithium electrode. The capacity associated with the EDL is comparable for both systems (Figure 7b). However, the diffusion parameter increases exponentially during intercalation for the hybrid system, while it remains almost unchanged for the half-cell (Figure 7f). This suggests that the reaction occurring at the positive electrode influences ion diffusion at the negative electrode. Likely, during the reaction at the positive electrode, lithium ions are released, which diffuse towards the negative electrode, contributing to the intercalation process. The time constant value in the initial phase is comparable for both systems (Figure 7g), but later it increases for the hybrid system, also suggesting interference in SEI formation. However, after the SEI layer formation, the situation reverses, and the hybrid system is characterized by lower time constant values, meaning ions move faster, confirming the relationship obtained in the diffusion parameter calculations. Overall, the presence of oxidation reactions at the positive electrode results in better ion diffusion in the electrolyte and facilitated lithium-ion intercalation. Comparing the obtained relationships of individual capacity parameters, there is no significant difference. Only in the hybrid system is there a slightly higher contribution of redox capacity, likely due to SEI layer buildup. It is also worth noting the difference in total capacity, which is nearly

Research Article
doi.org/10.1002/batt.202400822
Chemistry Europe
European Chemical Societies Publishing

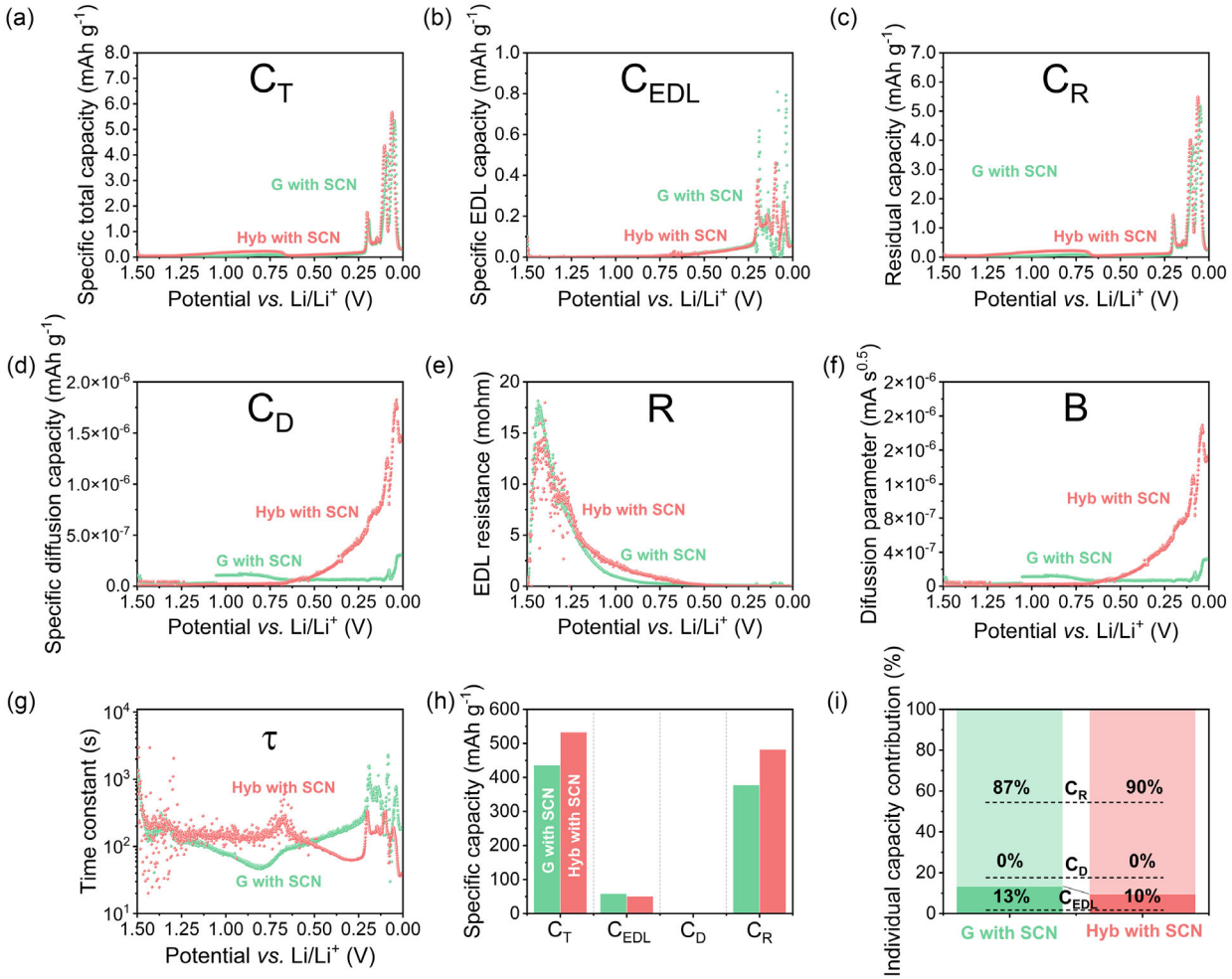

Figure 7. SPECS results of half-cell and full-cell using graphite with thiocyanate salt as an electrolyte additive a) specific total capacity (C_T), b) specific EDL capacity (C_{EDL}), c) residual capacity (C_R), d) specific diffusion capacity (C_D), e) EDL resistance (R), f) diffusion parameter (B), g) time constant (τ), h) specific capacity comparison, and i) individual capacity contribution.

100 mAh g^{-1}. This difference is due to the SEI layer buildup, as the intercalation curves of both systems overlap (Figure S6a). In the galvanostatically charged system, there was no such difference in capacity values. Therefore, this increase in capacity mainly results from the prolonged duration of the SPECS study. In this case, thiocyanates have more time to react at the positive electrode, leading to greater overall capacity. Therefore, the numerical values for capacity obtained by the SPECS technique should be considered indicative.

After conducting research using the SPECS technique, it was decided to compare the results using the GITT technique. For this purpose, all previously assembled systems were examined by applying 1 h of charging and 1 h of resting, and the results are presented in **Figure 8**. The applied current corresponded to a C/20 rate.

Figure 8a shows the GITT results for the half-cell with AC with and without the addition of thiocyanates. As shown, the system without thiocyanates quickly reaches the cutoff potential limit of the positive electrode. The system with thiocyanates, however, exhibits a visible plateau at a potential value of ≈3.5 V, after which it reaches the maximum potential significantly later than the system without SCN, which is consistent with the galvanostatic studies (Figure 3a). Based on the obtained potential dependence over time, the diffusion coefficient of these systems was calculated and presented in Figure 8b. An increased diffusion was observed in the initial phase, followed by a *plateau*. Interestingly, the results do not coincide with those obtained using the SPECS technique, where the thiocyanate reaction influenced the diffusion parameter value. It should be noted, however, that the diffusion coefficient (m^2 s^{-1}) calculated using GITT is one of the components of the equation for the diffusion parameter (mA s^{-1}) calculated in SPECS. Similar values should not be expected, but a proportional response should be. It is worth mentioning that the charging time of the half-cells was significantly longer than anticipated. This occurs due to the self-discharge of the positive electrode, making the GITT technique not the best for studying systems with AC.

Next, graphite half-cells with and without thiocyanate addition were examined (Figure 8c). In this case, as shown in Figure 3b, very similar performance of both systems was obtained, with the only difference being a slightly larger irreversible capacity associated with SEI formation in the SCN cell.

Research Article
doi.org/10.1002/batt.202400822
Chemistry Europe
European Chemical Societies Publishing

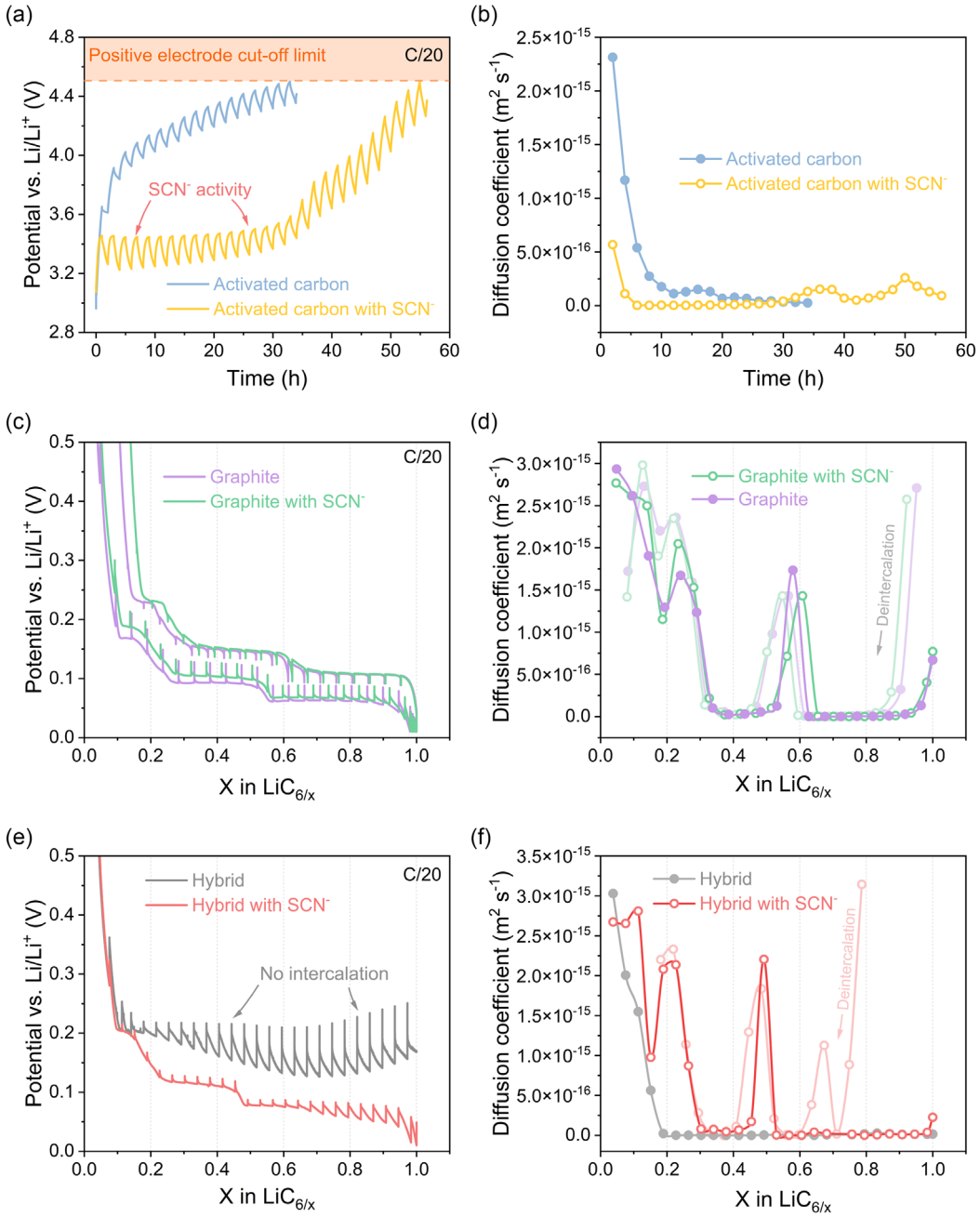

Figure 8. GITT results of half cells a) with activated carbon, c) with graphite, e) graphite in full cells, and b,d,f) calculated diffusion coefficients based on these results.

The calculated diffusion coefficient values are characteristic of graphite systems with distinctly marked intercalation stages. The results of both systems overlap, suggesting similar electrochemical performance. However, in this case, the diffusion coefficient curve aligns with the results obtained using the SPECS technique (Figure 5f), where responses related to intercalation stages can also be observed in the same manner.

Subsequently, full hybrid systems with and without SCN salt addition were examined (Figure 8e). As confirmed by previous studies, the system without thiocyanates did not reach the target potential value (0.01 V), thus not fully intercalating. The diffusion coefficient value confirms the lack of intercalation stages, with ion movement occurring only in the initial phase, and later the diffusion coefficient being close to zero. In the case of the hybrid with SCN, the graphite electrode was correctly intercalated, and the very low potential changes during electrode resting suggest that the electrode "held" the potential better than graphite intercalated in the half-cell. This phenomenon is likely due to a more tightly formed SEI layer due to the reaction occurring at the positive electrode. In the case of the diffusion coefficient, distinct intercalation stages are visible, but they are shifted, i.e., they occur earlier than in the case of graphite intercalated in half-cells. Comparing the diffusion coefficient results with those from the SPECS technique shows

a similarity in the curve's character, the intercalation stages are also visible. However, in the case of GITT, the diffusion value between the intercalation stages is practically zero, while in SPECS, it is increasing. Both techniques provide similar, yet not identical results. This suggests that to fully understand the system characteristics, multiple techniques should be used, as there is no single universal solution.

4. Conclusions

This study has presented a detailed analysis of the effects of LiSCN as a redox-active additive in the electrolyte of LICs. The use of SPECS and GITT techniques provided comprehensive insights into the electrochemical behaviour of the system. In the studied conditions, the thiocyanate reaction proceeds with an efficiency of ≈81%, resulting in a capacity of 301 mAh g^{-1} for the positive electrode. Nevertheless, a portion of the remaining capacity remains within the system, with part of it (11 mAh g^{-1}) being utilized for the formation of the SEI layer. Notably, the presence of thiocyanates significantly reduces the resistance of the negative electrode by 30%. The addition of LiSCN facilitated effective prelithiation, enhancing the capacity and performance of the graphite negative electrode. SPECS analysis showed distinct intercalation stages and improved ion diffusion in hybrid systems, while GITT confirmed these findings through characteristic diffusion coefficients. The results indicate that redox-active electrolytes, specifically those containing LiSCN, significantly enhance LIC performance by promoting better lithium intercalation and reducing electrode resistance. This study underscores the potential of redox-active additives in developing high-performance LICs, contributing to advancements in energy storage technology for automotive, renewable energy, and portable electronics applications.

Acknowledgements

This work was financially supported by the European Research Council within the Proof of Concept project (GA 101138710) under European Union Horizon Europe Research and Innovation programme. The work of Przemyslaw Galek was supported by the European Research Council under the European Union's Horizon Europe Research and Innovation Programme (grant agreement no. 101054940; title: Ultracapacitor Logic Gates).

Open Access funding enabled and organized by Projekt DEAL.

Conflict of Interest

The authors declare no conflict of interest.

Data Availability Statement

The data that support the findings of this study are available from the corresponding author upon reasonable request.

Keywords: galvanostatic intermittent titration techniques · ion diffusion · lithium thiocyanate · lithium-ion capacitors · one-step pre-intercalation · step potential electrochemical spectroscopy

[1] P. Simon, Y. Gogotsi, *Nat. Mater.* **2020**, *19*, 1151.
[2] P. Y. Hung, H. H. Zhang, H. Lin, Q. S. Guo, K. T. Lau, B. H. Jia, *J. Energy Chem.* **2022**, *68*, 580.
[3] R. T. Yadlapalli, R. R. Alla, R. Kandipati, A. Kotapati, *J. Energy Storage* **2022**, *49*, 104194.
[4] P. Drabek, L. Streit, 2009 IEEE Vehicle Power and Propulsion Conf, Dearborn, MI, USA IEEE, **2009**, pp. 1826–1830.
[5] J. T. Frith, M. J. Lacey, U. Ulissi, *Nat. Commun.* **2023**, *14*, 420.
[6] J. Zhao, A. F. Burke, *Adv. Energy Mater.* **2020**, *11*, 2002192.
[7] A. Manthiram, *ACS Cent. Sci.* **2017**, *3*, 1063.
[8] T. Kim, W. T. Song, D. Y. Son, L. K. Ono, Y. B. Qi, *J. Mater. Chem. A* **2019**, *7*, 2942.
[9] P. Jezowski, O. Crosnier, E. Deunf, P. Poizot, F. Beguin, T. Brousse, *Nat. Mater.* **2018**, *17*, 167.
[10] M. Soltani, S. H. Beheshti, *J. Energy Storage* **2021**, *34*, 102019.
[11] M. H. Nazir, A. Rahil, E. Partenie, M. Bowkett, Z. A. Khan, M. M. Hussain, S. Z. J. Zaidi, *Battery Energy* **2022**, *1*, 20220022.
[12] M. Uno, K. Tanaka, *IEEE Trans. Aerosp. Electron. Syst.* **2013**, *49*, 175.
[13] S. Barcellona, F. Ciccarelli, D. Iannuzzi, L. Piegari, *Electr. Power Compo. Syst.* **2016**, *44*, 1248.
[14] V. Khomenko, V. Barsukov, *Mater. Today-Proc.* **2019**, *6*, 116.
[15] G. Kothandam, G. Singh, X. Guan, J. M. Lee, K. Ramadass, S. Joseph, M. Benzigar, A. Karakoti, J. Yi, P. Kumar, A. Vinu, *Adv. Sci.* **2023**, *10*, e2301045.
[16] Y. Yao, H. Cumberbatch, D. D. Robertson, M. A. Chin, R. Lamkin, S. H. Tolbert, *Adv. Funct. Mater.* **2023**, *34*, 2304896.
[17] X. J. Wang, L. L. Liu, Z. Q. Niu, *Mater. Chem. Front.* **2019**, *3*, 1265.
[18] S. Jayaraman, A. Jain, M. Ulaganathan, E. Edison, M. P. Srinivasan, R. Balasubramanian, V. Aravindan, S. Madhavi, *Chem. Eng. J.* **2017**, *316*, 506.
[19] R. T. Wang, J. W. Lang, P. Zhang, Z. Y. Lin, X. B. Yan, *Adv. Funct. Mater.* **2015**, *25*, 2270.
[20] T. Insinna, E. N. Bassey, K. Marker, A. Collauto, A. L. Barra, C. P. Grey, *Chem. Mater.* **2023**, *35*, 5497.
[21] O. E. Eleri, F. L. Lou, Z. X. Yu, *Batteries-Basel* **2023**, *9*, 533.
[22] J. H. Lee, W. H. Shin, S. Y. Lim, B. G. Kim, J. W. Choi, *Mater. Renewable Sustainable* **2014**, *3*, 1.
[23] S. Zhang, C. Li, X. Zhang, X. Sun, K. Wang, Y. Ma, *ACS Appl. Mater. Interfaces* **2017**, *9*, 17136.
[24] A. Platek-Mielczarek, J. Conder, K. Fic, C. M. Ghimbeu, *J. Power Sources* **2022**, *542*, 231714.
[25] S. D. Magar, C. Leibing, J. L. Gómez-Urbano, R. Cid, D. Carriazo, A. Balducci, *Electrochim. Acta* **2023**, *446*, 142104.
[26] L. M. Jin, C. Shen, A. Shellikeri, Q. Wu, J. S. Zheng, P. Andrei, J. G. Zhang, J. P. Zheng, *Energy Environ. Sci.* **2020**, *13*, 2341.
[27] T. Aida, K. Yamada, M. Morita, *Electrochem. Solid State* **2006**, *9*, A534.
[28] C. Decaux, G. Lota, E. Raymundo-Piñero, E. Frackowiak, F. Béguin, *Electrochim. Acta* **2012**, *86*, 282.
[29] A. Maćkowiak, P. Jeżowski, Y. Matsui, M. Ishikawa, K. Fic, *Energy Storage Mater.* **2024**, *65*, 103163.
[30] S. S. Zhang, *J. Power Sources* **2006**, *162*, 1379.
[31] S. Bolloju, N. Vangapally, Y. Elias, S. Luski, N.-L. Wu, D. Aurbach, *Prog. Mater. Sci.* **2025**, *147*, 101349.
[32] L. Wang, F. Wu, Y. Yao, C. Zhang, *ChemElectroChem* **2024**, *11*, e202400019.
[33] E. Barsoukov, J. R. Macdonald, *Impedance Spectroscopy: Theory, Experiment, and Applications*, John Wiley & Sons, Incorporated, Hoboken **2005**.
[34] L. Demarconnay, E. Raymundo-Piñero, F. Béguin, *J. Power Sources* **2011**, *196*, 580.
[35] H. M. Fellows, M. Forghani, O. Crosnier, S. W. Donne, *J. Power Sources* **2019**, *417*, 193.
[36] P. Galek, A. Mackowiak, P. Bujewska, K. Fic, *Front. Energy Res.* **2020**, *8*, 139.
[37] B. Babu, P. Simon, A. Balducci, *Adv. Energy Mater.* **2020**, *10*, 2001128.
[38] M. D. Levi, E. A. Levi, D. Aurbach, *J. Electroanal. Chem.* **1997**, *421*, 89.
[39] J. H. Park, H. Yoon, Y. Cho, C. Y. Yoo, *Materials* **2021**, *14*, 4683.

[40] A. Nickol, T. Schied, C. Heubner, M. Schneider, A. Michaelis, M. Bobeth, G. Cuniberti, *J. Electrochem. Soc.* **2020**, *167*, 90546.
[41] M. F. Dupont, S. W. Donne, *Electrochim. Acta* **2015**, *167*, 268.
[42] M. F. Dupont, S. W. Donne, *J. Electrochem. Soc.* **2016**, *163*, A888.
[43] A. Maćkowiak, P. Galek, P. Jeżowski, K. Fic, *Electrochim. Acta* **2023**, *463*, 142796.
[44] K. Fic, A. Platek, J. Piwek, E. Frackowiak, *Mater. Today* **2018**, *21*, 437.
[45] M. Forghani, S. W. Donne, *J. Electrochem. Soc.* **2018**, *165*, A593.
[46] M. Forghani, H. Mavroudis, J. McCarthy, S. W. Donne, *Electrochim. Acta* **2020**, *332*, 135508.
[47] M. Forghani, S. W. Donne, *J. Electrochem. Soc.* **2018**, *165*, A664.
[48] W. Weppner, R. A. Huggins, *J. Electrochem. Soc.* **2019**, *124*, 1569.
[49] B. A. Mei, J. Lau, T. Lin, S. H. Tolbert, B. S. Dunn, L. Pilon, *J. Phys. Chem. C* **2018**, *122*, 24499.

Manuscript received: December 30, 2024
Revised manuscript received: April 7, 2025
Version of record online: April 17, 2025